PROBING PHOTONIC CONTENT OF THE PROTON USING PHOTON-INDUCED DILEPTON PRODUCTION IN p+Pb COLLISIONS AT THE LHC*

M. Łuszczak

Faculty of Mathematics and Natural Sciences, University of Rzeszów
Pigonia 1, 35-310 Rzeszów, Poland

M. Dyndal

CERN, Geneva, Switzerland

A. Glazov

Deutsches Elektronen-Synchrotron DESY, Hamburg, Germany

R. Sadykov

Joint Institute for Nuclear Research (JINR), Dubna, Russia

(Received April 24, 2019)

We propose a new experimental method to probe the photon–parton distribution function inside the proton (photon PDF) at the LHC energies. The method is based on the measurement of dilepton production from the $\gamma p \to \ell^+\ell^- + X$ reaction in proton–lead collisions. We firstly calculate the cross sections for this process with collinear photon PDFs, where we identify optimal choice of the scale, in analogy to deep inelastic scattering kinematics. We then perform calculations including the transverse-momentum dependence of the probed photon. Finally, we estimate rates of the process for the existing LHC data samples.

DOI:10.5506/APhysPolB.50.1117

1. Introduction

A significant fraction of proton–proton (pp) collisions at the LHC involves quasi-real photon interactions. Precise calculations of various electroweak reactions in pp collisions at the LHC need to account for, on top of the higher-order corrections, the effects of photon-induced processes. The

* Presented at the Cracow Epiphany Conference on Advances in Heavy Ion Physics, Kraków, Poland, January 8–11 2019.

relevant examples are the production of lepton pairs [1–5] or pairs of electroweak bosons [6–9]. The approach, proposed in Ref. [10], provides a model-independent determination of the photon PDF (embedded in the so-called LUXqed distribution), and it is based on proton structure function and elastic form factor fits in electron–proton scattering. Up to date, there are no experimentally clean processes identified that would allow to either strongly constrain or verify the calculations. For example, the extraction of photon PDF from isolated photon production in deep inelastic scattering (DIS) [11] or from inclusive $pp \to \ell^+\ell^- + X$ reaction [2, 12, 13] is limited due to the large QCD background. On the contrary, the elastic part of the photon PDF is verified via exclusive $\gamma\gamma \to \ell^+\ell^-$ process, measured in pp collisions by ATLAS [14, 15], CMS [16, 17] and, recently, by CMS+TOTEM [18] collaborations.

We, therefore, propose a new experimental method to constrain photonic content of the proton. Thanks to the large fluxes of quasi-real photons from the lead ion (Pb) at the LHC, the photon-induced dilepton production in p + Pb collision configuration is a very clean way to probe photon PDF inside a proton. This process is schematically shown in Fig. 1, where by analogy to DIS, two leading-order diagrams can be identified. Since the photon flux from the ion scales with Z^2 and QCD-induced cross-sections scale approximately with A, the amount of QCD background is greatly reduced comparing to the pp case.

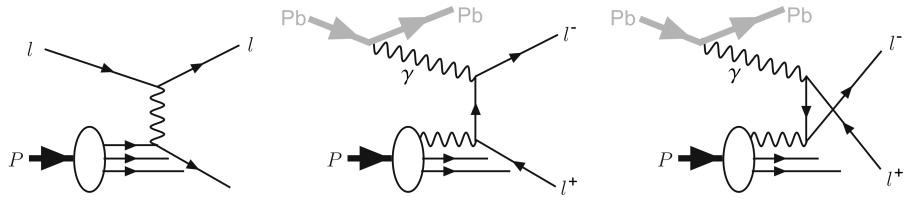

Fig. 1. Schematic graphs for deep inelastic scattering, $\ell^\pm p \to \ell^\pm + X$ (a) and photon-induced dilepton prodcution, $\gamma p \to \ell^+\ell^- + X$, in p + Pb collisions for t-channel (b) and u-channel (c) lepton exchange.

2. Sketch of the formalism

2.1. Elastic photon fluxes

Elastic contribution for the $\gamma p \to \ell^+\ell^- + X$ reaction is obtained as

$$\gamma_{\rm el}^{p}\left(x, Q^2\right) = \frac{\alpha_{\rm em}}{\pi}\left[\left(1-\frac{x}{2}\right)^2 \frac{4m_p^2 G_{\rm E}^2\left(Q^2\right) + Q^2 G_{\rm M}^2\left(Q^2\right)}{4m_p^2 + Q^2} + \frac{x^2}{4} G_{\rm M}^2\left(Q^2\right)\right], \tag{1}$$

where x is the momentum fraction of the proton taken by the photon, Q^2 is the photon virtuality, $\alpha_{\rm em}$ is the electromagnetic structure constant, m_p is the proton mass, $G_{\rm E}(Q^2)$ is the electric and $G_{\rm M}(Q^2)$ is magnetic form factors of the proton.

To express the elastic photon flux for the nucleus ($\gamma_{\rm el}^{\rm Pb}$), we follow Ref. [19] and replace

$$\frac{4m_p^2 G_{\rm E}^2\left(Q^2\right) + Q^2 G_{\rm M}^2\left(Q^2\right)}{4m_p^2 + Q^2} \longrightarrow Z^2 F_{\rm em}^2\left(Q^2\right) , \tag{2}$$

where $F_{\rm em}(Q^2)$ is the electromagnetic form factor of the nucleus and Z is its charge. We also neglect the magnetic form factor of the ion in the following.

For the Pb nucleus, we use the form factor parameterization from the STARlight MC generator [20]

$$F_{\rm em}\left(Q^2\right) = \frac{3}{(QR_A)^3}\left[\sin(QR_A) - QR_A\cos(QR_A)\right]\frac{1}{1+a^2Q^2} , \tag{3}$$

where $R_A = 1.1A^{1/3}$ fm, $a = 0.7$ fm and $Q = \sqrt{Q^2}$.

2.2. Collinear-factorization approach

In the collinear approach, the $p + {\rm Pb} \to {\rm Pb} + \ell^+\ell^- + X$ production cross section can be written as

$$\sigma = S^2 \int {\rm d}x_p\, {\rm d}x_{\rm Pb} \left[\left(\gamma_{\rm el}^p(x_p) + \gamma_{\rm inel}^p\left(x_p, \mu^2\right)\right)\gamma_{\rm el}^{\rm Pb}(x_{\rm Pb})\sigma_{\gamma\gamma\to\ell^+\ell^-}(x_p, x_{\rm Pb})\right] , \tag{4}$$

where $\sigma_{\gamma\gamma\to\ell^+\ell^-}$ is the elementary cross section for the $\gamma\gamma \to \ell^+\ell^-$ subprocess and S^2 is the so-called survival factor which takes into account the requirement that there be no hadronic interactions between the proton and the ion.

2.3. $k_{\rm T}$-factorization approach

In the $k_{\rm T}$-factorization approach, one can parametrize the $\gamma^* p \to X$ vertices in terms of the proton structure functions. The photons from inelastic production have transverse momenta and non-zero virtualities Q^2, and the unintegrated photon distributions are used, in contrast to collinear distributions. In the DIS limit, the unintegrated inelastic photon flux can be obtained using the following equation [4, 21]:

$$\gamma_{\rm inel}^p(x, \vec{q}_{\rm T}) = \frac{1}{x}\frac{1}{\pi\vec{q}_{\rm T}^2}\int\limits_{M_{\rm thr}^2} {\rm d}M_X^2 \mathcal{F}_{\gamma^*\leftarrow p}^{\rm in}\left(x, \vec{q}_{\rm T}, M_X^2\right) , \tag{5}$$

and we use the functions $\mathcal{F}_{\gamma^*\leftarrow p}^{\rm in}$ from [9, 19]

$$\mathcal{F}^{\rm in}_{\gamma^*\leftarrow p}(x,\vec{q}_{\rm T}) = \frac{\alpha_{\rm em}}{\pi}\left\{(1-x)\left(\frac{\vec{q}^{\,2}_{\rm T}}{\vec{q}^{\,2}_{\rm T}+x\left(M_X^2-m_p^2\right)+x^2m_p^2}\right)^2 \times\frac{F_2\left(x_{\rm Bj},Q^2\right)}{Q^2+M_X^2-m_p^2}+\frac{x^2}{4x_{\rm Bj}^2}\frac{\vec{q}^{\,2}_{\rm T}}{\vec{q}^{\,2}_{\rm T}+x\left(M_X^2-m_p^2\right)+x^2m_p^2}\frac{2x_{\rm Bj}F_1\left(x_{\rm Bj},Q^2\right)}{Q^2+M_X^2-m_p^2}\right\}.$$

The virtuality Q^2 of the photon depends on the photon transverse momentum ($\vec{q}^{\,2}_{\rm T}$) and the proton remnant mass (M_X)

$$Q^2 = \frac{\vec{q}^{\,2}_{\rm T}+x\left(M_X^2-m_p^2\right)+x^2m_p^2}{(1-x)}. \tag{6}$$

Moreover, the proton structure functions $F_1(x_{\rm Bj},Q^2)$ and $F_2(x_{\rm Bj},Q^2)$ require the argument

$$x_{\rm Bj} = \frac{Q^2}{Q^2+M_X^2-m_p^2}. \tag{7}$$

Note that in Eq. (5) instead of using $F_2(x_{\rm Bj},Q^2), F_1(x_{\rm Bj},Q^2)$, we in practise use the pair $F_2(x_{\rm Bj},Q^2)$, $F_{\rm L}(x_{\rm Bj},Q^2)$, where

$$F_{\rm L}\left(x_{\rm Bj},Q^2\right) = \left(1+\frac{4x_{\rm Bj}^2m_p^2}{Q^2}\right)F_2\left(x_{\rm Bj},Q^2\right)-2x_{\rm Bj}F_1\left(x_{\rm Bj},Q^2\right) \tag{8}$$

is the longitudinal structure function of the proton.

These unintegrated photon fluxes enter the $p+{\rm Pb}\to{\rm Pb}+\ell^+\ell^-+X$ production cross section as

$$\sigma = S^2\int {\rm d}x_p\,{\rm d}x_{\rm Pb}\,{\rm d}\vec{q}_{\rm T} \times\left[\left(\gamma^p_{\rm el}(x_p,\vec{q}_{\rm T})+\gamma^p_{\rm inel}(x_p,\vec{q}_{\rm T})\right)\gamma^{\rm Pb}_{\rm el}(x_{\rm Pb})\sigma_{\gamma^*\gamma\to\ell^+\ell^-}(x_p,x_{\rm Pb},\vec{q}_{\rm T})\right], \tag{9}$$

where $\sigma_{\gamma^*\gamma\to\ell^+\ell^-}$ is the off-shell elementary cross section [21] and for $x_p\ll 1$, we have $Q^2\approx\vec{q}^{\,2}_{\rm T}$ (see Eq. (6)). One should note that while the fluxes do not depend on the direction of $\vec{q}_{\rm T}$, averaging over directions of $\vec{q}_{\rm T}$ in the off-shell cross section replaces the average over photon polarizations in the collinear case.

3. Results

The results for the elastic case are cross-checked with the calculation from STARlight MC and good agreement between the fiducial cross sections is found: $\sigma_{\rm fid}^{\rm el} = 17.5$ nb, whereas $\sigma_{\rm fid}^{\rm STARlight} = 17.0$ nb. Both calculations are also corrected by a factor $S^2 = 0.96$ which is calculated using STARlight, where the hard-sphere proton–nucleus requirement [20] is used.

For the inelastic case ($\gamma p \to \ell^+\ell^- + X$), several recent parameterizations of the photon parton distributions are studied. All predictions are scaled by $S^2 = 0.95$, again derived from STARlight. This value of S^2 is lower than for the purely elastic case, due to slightly smaller average impact parameter between the proton and the ion in the inelastic reaction. One should note that all of these PDF sets include both elastic and inelastic parts of the photon spectrum.

The integrated fiducial cross sections for $p + \mathrm{Pb} \to \mathrm{Pb} + \ell^+\ell^- + X$ production at $\sqrt{s_{NN}} = 8.16$ TeV for different collinear photon PDF sets are summarized in Table I.

TABLE I

Integrated fiducial cross sections for $p + \mathrm{Pb} \to \mathrm{Pb} + \ell^+\ell^- + X$ production at $\sqrt{s_{NN}} = 8.16$ TeV for different collinear photon PDF sets. The effect of applying only $p_{\rm T}^{\ell}$ requirement is shown in the second column. The uncertainties denote the PDF uncertainties (if available) calculated at 68% C.L. For comparison, the cross section for purely elastic contribution is also shown.

Contribution	$p_{\rm T}^{\ell} > 4$ GeV	$p_{\rm T}^{\ell} > 4$ GeV, $\lvert\eta^{\ell}\rvert < 2.4$ $m_{\ell^+\ell^-} > 10$ GeV
$\gamma_{\rm el}^{p}$	44.9 nb	17.5 nb
$\gamma_{\rm el}^{p} + \gamma_{\rm inel}^{p}$ [CT14qed_inc]	98 ± 4 (PDF) nb	40 ± 2 (PDF) nb
$\gamma_{\rm el}^{p} + \gamma_{\rm inel}^{p}$ [LUXqed17]	105.8 ± 0.2 (PDF) nb	44.1 ± 0.1 (PDF) nb
$\gamma_{\rm el}^{p} + \gamma_{\rm inel}^{p}$ [NNPDF3.1luxQED]	115.6 ± 0.6 (PDF) nb	45.9 ± 0.3 (PDF) nb
$\gamma_{\rm el}^{p} + \gamma_{\rm inel}^{p}$ [HKR16qed]	121.6 nb	49.4 nb

Comparison of several lepton kinematic distributions between different photon-PDFs is shown in figure 2, including invariant mass and rapidity of lepton pair, and single-lepton transverse momentum/pseudorapidity distributions.

All photon PDF parameterizations agree within 10% with each other. The small differences are mainly due to overall PDF normalization, as no variation in the shape of various kinematic distributions is observed.

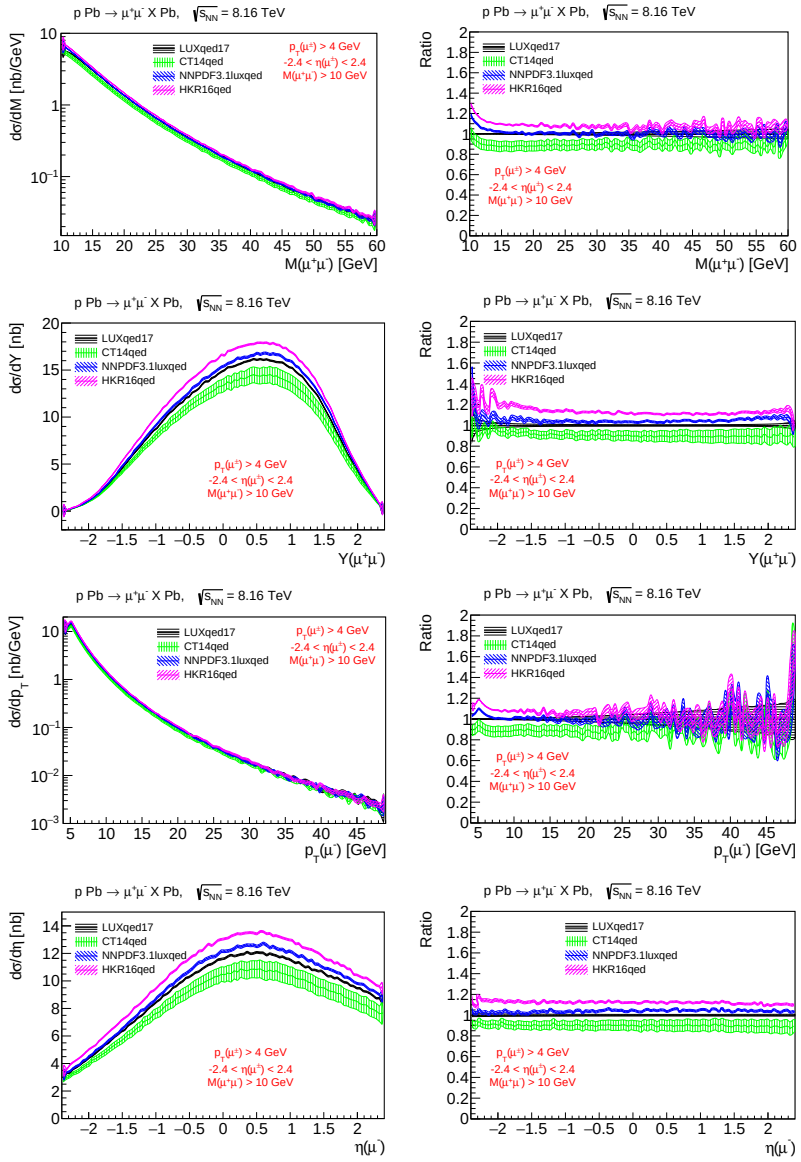

Fig. 2. Differential cross sections in the fiducial region for $p+\mathrm{Pb} \to \mathrm{Pb}+\ell^+\ell^-+X$ production at $\sqrt{s_{NN}} = 8.16$ TeV for different collinear photon PDF sets. Four differential distributions are shown (from top to bottom): invariant mass of lepton pair, pair rapidity, transverse momentum of negatively-charged lepton and its pseudorapidity. Figures on the right show the ratios to LUXqed17 PDF. The bands denote the PDF uncertainties (if available) calculated at 68% C.L., and the statistical uncertainties of the calculations added in quadrature.

Table II shows the comparison of integrated fiducial cross sections for inelastic $p + \mathrm{Pb} \to \mathrm{Pb} + \ell^+\ell^- + X$ production at $\sqrt{s_{NN}} = 8.16$ TeV for different proton structure functions used. All structure functions provide similar fiducial cross section at the level of 16–18 nb. These inelastic cross sections are also similar in size to the elastic contribution (18 nb) and are slightly lower than the numbers from collinear analysis, subtracted for elastic part (see Table I). A comparison is also made with LUX-like parametrization when the longitudinal structure function (F_L) is explicitly considered. This leads to the decrease of the cross section by 2%, similarly as in Ref. [9].

TABLE II

Integrated fiducial cross sections for inelastic $p+\mathrm{Pb} \to \mathrm{Pb}+\ell^+\ell^-+X$ production at $\sqrt{s_{NN}} = 8.16$ TeV for different proton structure functions. The effect of applying only p_T^ℓ requirement is shown in the second column.

Contribution	$p_\mathrm{T}^\ell > 4$ GeV	$p_\mathrm{T}^\ell > 4$ GeV, $\lvert\eta^\ell\rvert < 2.4$ $m_{\ell^+\ell^-} > 10$ GeV
γ^p_el	47.9 nb	18.3 nb
γ^p_inel [LUX-like F_2]	43.6 nb	17.4 nb
γ^p_inel [LUX-like $F_2 + F_\mathrm{L}$]	42.6 nb	17.1 nb
γ^p_inel [ALLM97 F_2]	41.7 nb	16.4 nb
γ^p_inel [SU F_2]	41.7 nb	16.7 nb
γ^p_inel [SY F_2]	40.4 nb	16.0 nb

Figure 3 presents differential cross sections for several lepton kinematic distributions: invariant mass of lepton pair, leading lepton transverse momentum, lepton pseudorapidity difference and leading lepton pseudorapidity. The shapes of the distributions obtained with various proton structure functions are very similar. For completeness, differential cross sections as a function of lepton pair transverse momentum and azimuthal angle difference between the pair are shown in figure 4. Quite large (small) transverse momenta (angle differences) are possible, in contrast to leading-order calculations with collinear photons where the corresponding distributions are just a Dirac delta functions.

Based on figure 4, it is also possible to separate experimentally the elastic part ($p + \mathrm{Pb} \to p + \mathrm{Pb} + \ell^+\ell^-$) with striking back-to-back topology, out of the inelastic contribution. With k_T-factorization, one can also calculate the mass of the proton remnants (M_X). This is shown in figure 5, where in contrary to the elastic case ($M_X = m_p$), quite large masses of the remnant system can be achieved.

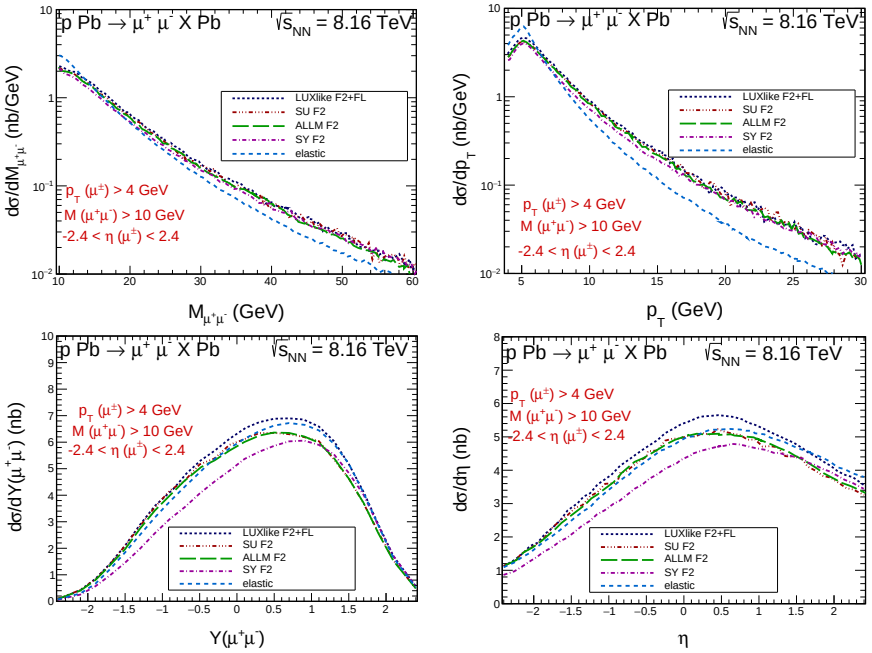

Fig. 3. Differential cross sections in the fiducial region for $p + \mathrm{Pb} \to \mathrm{Pb} + \ell^+\ell^- + X$ production at $\sqrt{s_{NN}} = 8.16$ TeV in the k_T-factorization approach for several proton structure functions. Four differential distributions are shown: invariant mass of lepton pair (top left), leading lepton transverse momentum (top right), dilepton rapidity (bottom left) and leading lepton pseudorapidity (bottom right). For comparison, the elastic contribution ($p + \mathrm{Pb} \to p + \mathrm{Pb} + \ell^+\ell^-$) is also shown.

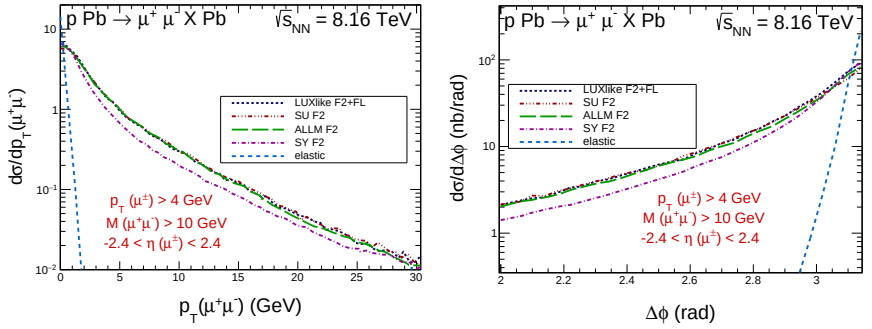

Fig. 4. Differential cross sections in the fiducial region for $p + \mathrm{Pb} \to \mathrm{Pb} + \ell^+\ell^- + X$ production at $\sqrt{s_{NN}} = 8.16$ TeV in the k_T-factorization approach for several proton structure functions. Two differential distributions are shown: transverse momentum of lepton pair (left) and azimuthal angle difference between the pair (right). For comparison, the elastic contribution ($p + \mathrm{Pb} \to p + \mathrm{Pb} + \ell^+\ell^-$) is also shown.

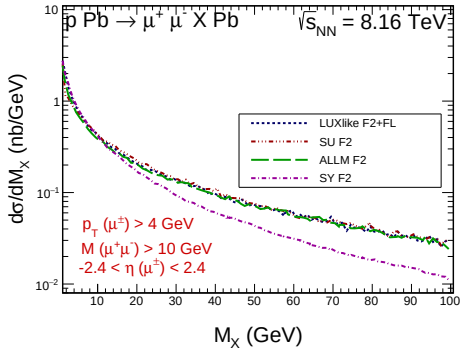

Fig. 5. Differential cross section as a function of the mass of the proton remnants in the fiducial region for $p+\mathrm{Pb} \to \mathrm{Pb}+\ell^+\ell^- + X$ production at $\sqrt{s_{NN}} = 8.16$ TeV in the k_T-factorization approach for several proton structure functions.

Table III shows the expected number of events for $p + \mathrm{Pb} \to \mathrm{Pb} + \ell^+\ell^- + X$ production at $\sqrt{s_{NN}} = 8.16$ TeV and configuration described above. Approximately 2500 elastic dilepton events are expected. Depending on the calculations, 3400 (collinear with LUXqed17 PDF) or 2400 (k_T factorization with LUX-like $F_2 + F_\mathrm{L}$) reconstructed inelastic events are predicted. The data should be, therefore, sensitive to discrimination between the predictions based on collinear and k_T-factorization approaches, using existing datasets collected by ATLAS and CMS.

TABLE III

Expected number of events for $p + \mathrm{Pb} \to \mathrm{Pb} + \ell^+\ell^- + X$ production at $\sqrt{s_{NN}} = 8.16$ TeV assuming $\int L\,\mathrm{d}t = 200$ nb^{-1}. Shown are several contributions: purely elastic, inelastic with collinear LUXqed17 PDF and inelastic with k_T factorization and LUX-like $F_2 + F_\mathrm{L}$ proton structure function parameterization. An effect of possible experimental efficiencies is shown in the last column.

Contribution	Expected events ($C = 1$)	Expected events ($C = 0.7$)
γ^p_el	3600	2500
γ^p_inel [LUXqed17 collinear]	5600	3900
γ^p_inel [LUX-like $F_2 + F_\mathrm{L}$]	3400	2400

4. Conclusions

In summary, we propose a method that would allow to test and constrain the photon parton distribution at the LHC energies. This method is based on the measurement of the cross section for the reaction p+Pb $\to$ Pb+$\ell^+\ell^-$+X,

where the expected background is small comparing to the analogous process in pp collisions. Results are shown for different choices of collinear photon PDFs, and a comparison is made with unintegrated photon distributions that include non-zero photon transverse momentum. Due to the smearing of dilepton transverse momentum introduced by the k_{T}-factorization approach, these two approaches lead to the cross sections that differ by about 30%. Using simple (realistic) experimental requirements on lepton kinematics, it is shown that one can expect $O(3000)$ inelastic events with the existing datasets recorded by ATLAS/CMS at $\sqrt{s_{NN}} = 8.16$ TeV for each lepton flavour.

REFERENCES

[1] G. Aad *et al.* [ATLAS Collab.], *J. High Energy Phys.* **1406**, 112 (2014).
[2] G. Aad *et al.* [ATLAS Collab.], *J. High Energy Phys.* **1608**, 009 (2016).
[3] E. Accomando *et al.*, *Phys. Rev. D* **95**, 035014 (2017).
[4] M. Łuszczak, W. Schäfer, A. Szczurek, *Phys. Rev. D* **93**, 074018 (2016).
[5] L.A. Harland-Lang, V.A. Khoze, M.G. Ryskin, *Eur. Phys. J. C* **76**, 255 (2016).
[6] M. Luszczak, A. Szczurek, C. Royon, *J. High Energy Phys.* **1502**, 098 (2015).
[7] A. Denner, S. Dittmaier, M. Hecht, C. Pasold, *J. High Energy Phys.* **1602**, 057 (2016).
[8] M. Dyndal, L. Schoeffel, *Acta Phys. Pol. B* **47**, 1645 (2016).
[9] M. Łuszczak, W. Schäfer, A. Szczurek, *J. High Energy Phys.* **1805**, 064 (2018).
[10] A. Manohar, P. Nason, G.P. Salam, G. Zanderighi, *Phys. Rev. Lett.* **117**, 242002 (2016).
[11] C. Schmidt, J. Pumplin, D. Stump, C.P. Yuan, *Phys. Rev. D* **93**, 114015 (2016).
[12] R.D. Ball *et al.* [NNPDF Collab.], *Nucl. Phys. B* **877**, 290 (2013).
[13] F. Giuli *et al.* [xFitter Developers' Team], *Eur. Phys. J. C* **77**, 400 (2017).
[14] G. Aad *et al.* [ATLAS Collab.], *Phys. Lett. B* **749**, 242 (2015).
[15] M. Aaboud *et al.* [ATLAS Collab.], *Phys. Lett. B* **777**, 303 (2018).
[16] S. Chatrchyan *et al.* [CMS Collab.], *J. High Energy Phys.* **1201**, 052 (2012).
[17] S. Chatrchyan *et al.* [CMS Collab.], *J. High Energy Phys.* **1211**, 080 (2012).
[18] A.M. Sirunyan *et al.* [CMS and TOTEM collabs.], *J. High Energy Phys.* **1807**, 153 (2018).
[19] V.M. Budnev, I.F. Ginzburg, G.V. Meledin, V.G. Serbo, *Phys. Rep.* **15**, 181 (1975).
[20] S.R. Klein *et al.*, *Comput. Phys. Commun.* **212**, 258 (2017).
[21] G.G. da Silveira *et al.*, *J. High Energy Phys.* **1502**, 159 (2015).